

# Spatially-resolved control of fictitious magnetic fields in a cold atomic ensemble

ADAM LESZCZYŃSKI<sup>1</sup>, MATEUSZ MAZELANIK<sup>1</sup>, MICHAŁ LIPKA<sup>1</sup>, MICHAŁ PARNIAK<sup>1,\*</sup>, MICHAŁ DĄBROWSKI<sup>1</sup>, AND WOJCIECH WASILEWSKI<sup>1</sup>

<sup>1</sup>Institute of Experimental Physics, Faculty of Physics, University of Warsaw, Pasteura 5, 02-093 Warsaw, Poland

\*Corresponding author: [michal.parniak@fuw.edu.pl](mailto:michal.parniak@fuw.edu.pl)

Compiled August 24, 2021

**Effective and unrestricted engineering of atom-photon interactions requires precise spatially-resolved control of light beams. The significant potential of such manipulations lies in a set of disciplines ranging from solid state to atomic physics. Here we use a Zeeman-like ac-Stark shift of a shaped laser beam to perform rotations of spins with spatial resolution in a large ensemble of cold rubidium atoms. We show that inhomogeneities of light intensity are the main source of dephasing and thus decoherence, yet with proper beam shaping this deleterious effect is strongly mitigated allowing rotations of 15 rad within one spin-precession lifetime. Finally, as a particular example of a complex manipulation enabled by our scheme, we demonstrate a range of collapse-and-revival behaviours of a free-induction decay signal by imprinting comb-like patterns on the atomic ensemble.** © 2021 Optical Society of America

**OCIS codes:** (020.0020) Atomic and molecular physics; (020.6580) Stark effect.

<http://dx.doi.org/10.1364/ao.XX.XXXXXX>

The prospect of the all-optical arbitrary manipulation of spin drives both classical and quantum engineering [1, 2], as it could enable efficient quantum information processing, e.g. with single spins [3, 4], as well as dense and efficient storage of classical information [5]. Generation of fictitious magnetic fields [6] by an optically-induced vector ac-Stark shift is a viable way of performing such spin manipulations [2, 7], due to its inherently off-resonant and thus absorption-free nature. Moreover, application of fictitious magnetic fields to spin ensembles proves to be a feasible way to reach high sensitivities to real magnetic fields by means of all-optical methods [8–10]. Spatial control of the applied effective potential paves the way towards novel applications such as high spatial-resolution magnetometry [11], magnetic field imaging [12], magnetic gradiometry [13], super-resolved imaging [14] or implicitly generation of tunable gauge potentials on ultracold atoms [15]. Precise spatial control could also enable efficient operation of photon echos [16, 17] used in gradient-echo quantum memories [18, 19], precise atom manipulation [7, 20] as well as novel atom trapping techniques [21, 22]. New ways to engineer efficient nonlinear light-atom

interactions also arise as the spatial degree of freedom inherently encompasses phase-matching [23, 24], also in quantum memories [25–27].

In this Letter we demonstrate spatially-resolved control of a vector ac-Stark shift [28] on a cold rubidium ensemble. Using a phase-only spatial light modulator (SLM) we shape the spatial profile of an off-resonant laser pulse that induces the ac-Stark shift on the atoms. To characterize the interaction we observe the effect of the applied fictitious magnetic field on a free-induction decay (FID) signal [29, 30]. Furthermore, we demonstrate the importance of precise control of the ac-Stark field intensity and unambiguously verify that intensity inhomogeneities and resulting dephasing are the most important source of decoherence in our system. With appropriate corrections we apply a phase shift of over 15 rad within the lifetime of the spin coherence. This shows that a large variety of manipulations on spin-precession (traditionally denoted as FID) temporal dynamics are possible, ranging from simple frequency shifts, through inducing beat-notes, to rapid collapse-and-revival behavior. All of this confirms that our platform is a versatile tool to efficiently prepare complex spin patterns in the cold atomic ensemble.

To accurately describe observed experimental results let us introduce the basic theory of ac-Stark shift by considering the  $F = 1$  ground-state manifold of  $^{87}\text{Rb}$  atom, for which the Hamiltonian describing interaction with z-propagating laser beam can be decomposed into three components [28, 31, 32]:

$$\hat{H}_S = \hat{H}_S^{(0)} + \hat{H}_S^{(1)} + \hat{H}_S^{(2)} \quad (1)$$

with

$$\begin{aligned} \hat{H}_S^{(0)} &= \frac{2}{3} g \alpha^{(0)} \hat{S}_0, \\ \hat{H}_S^{(1)} &= g \alpha^{(1)} \hat{S}_z \hat{F}_z, \\ \hat{H}_S^{(2)} &= g \alpha^{(2)} \left[ \frac{1}{3} \hat{S}_0 (3 \hat{F}_z^2 - 2 \hat{1}) + \hat{S}_x (\hat{F}_x^2 - \hat{F}_y^2) + \hat{S}_y (\hat{F}_x \hat{F}_y + \hat{F}_y \hat{F}_x) \right], \end{aligned} \quad (2)$$

where:  $\alpha^{(i)}$  is the tensor of atomic polarizability depending on atomic quantum numbers and detuning  $\Delta$ ,  $g = \omega_0 / (2\epsilon_0 V)$  is a form factor [31] (with the resonant atomic frequency  $\omega_0$  and the interaction volume  $V$ ), and  $\hat{S}_j$  ( $\hat{F}_j$ ) are Stokes (atomic spin) operators [28, 31]. For detuning  $\Delta$  much bigger than the decay rate  $\Gamma$ , tensor part of the interaction  $\alpha^{(2)}$  is proportional to  $1/\Delta^2$ , while scalar  $\alpha^{(0)}$  and vector  $\alpha^{(1)}$  parts are proportional

to  $1/\Delta$  [28]. Furthermore, for strong circularly polarized light we have  $|\langle \hat{S}_z \rangle| \gg |\langle \hat{S}_x \rangle|, |\langle \hat{S}_y \rangle|$ . Therefore the contribution of  $\hat{H}_S^{(2)}$  can be neglected for large detuning  $\Delta$  and circular polarization. Moreover, the scalar part  $\hat{H}_S^{(0)}$  causes only constant shift of energy levels which does not affect the atomic spin dynamics.

In consequence the only part of the Hamiltonian  $\hat{H}_S$  (Eq. (1)) we need to consider is the vector term  $\hat{H}_S^{(1)}$ . Within the approximation of a classical electromagnetism, the form factor  $g$  obeys the relation:  $\hbar g \langle \hat{S}_z \rangle = qI / (2\epsilon_0 c)$ , where  $I$  is the light intensity and  $q = \pm 1$  corresponds to  $\sigma_{\pm}$  polarization of the ac-Stark-inducing laser beam, so the final form of the vector Hamiltonian is

$$\hat{H}_S^{(1)} = q \frac{\kappa}{\Delta} \frac{I}{2\hbar\epsilon_0 c} \hat{F}_z, \quad (3)$$

where  $\kappa = \alpha^{(1)}\Delta = \text{const.}$  for  $\Delta \gg \Gamma$ . This specific form is reminiscent of the Hamiltonian for an atom in an external magnetic field applied along the  $z$  direction, so we can define a fictitious magnetic field [6]:

$$\mathbf{B}_f = q \frac{1}{g_F \mu_B} \frac{\kappa}{\Delta} \frac{I}{2\hbar\epsilon_0 c} \hat{\mathbf{k}}, \quad (4)$$

where:  $\hat{\mathbf{k}} = \mathbf{k}/|\mathbf{k}|$  and  $\mathbf{k}$  – wavevector of the laser beam propagating along the  $z$  direction. When atomic ensemble is also influenced by a real magnetic field  $\mathbf{B}$ , taking into account all of the above approximations, the total Hamiltonian  $\hat{H}_S$  from Eq. (1) can be written in a traditional form:

$$\hat{H} = g_F \mu_B (\mathbf{B} + \mathbf{B}_f) \hat{\mathbf{F}}. \quad (5)$$

In consequence, atomic spins exposed to the ac-Stark beam precess around the effective magnetic field  $\mathbf{B}_{\text{eff}} = \mathbf{B} + \mathbf{B}_f$  with the Larmor frequency  $\omega_L = g_F \mu_B B_{\text{eff}} / \hbar$ .

The model presented here is derived neglecting incoherent excitation of atoms and subsequent re-emission of light, including the  $F = 2$  manifold. In the leading order of perturbation calculation the rate  $\Gamma_{\text{scatt}}$  of this incoherent scattering scales as

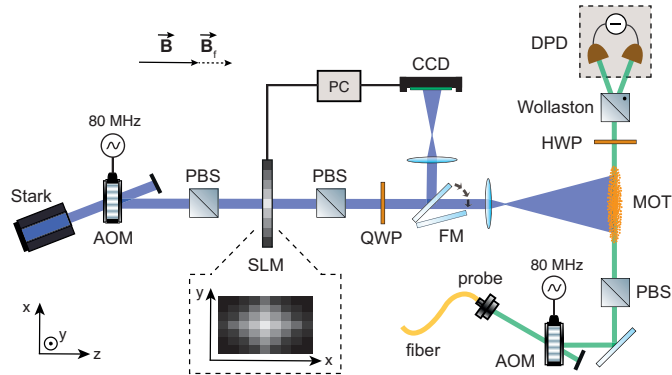


**Fig. 1.** Schematic of the experimental setup. Atoms released from the magneto-optical trap (MOT) are illuminated by two beams: linearly polarized probe and circularly polarized ac-Stark beam. ac-Stark beam intensity at the output of acousto-optic modulator (AOM) is shaped using reflective spatial light modulator (SLM), drawn in the transmission configuration for simplicity. Flip mirror (FM) switches SLM image between MOT and CCD camera. Differential photodiode (DPD) registers polarization rotation of the probe light. PBS, polarizing beamsplitter; HWP (QWP), half-wave (quarter-wave) plate.

$\Gamma_{\text{scatt}} \sim 1/\Delta^2$  [18]. Therefore, in the far-detuned regime of our experiment ( $\Delta \gg \Gamma$ ) we expect this contribution to be insignificant.

In our experiment, presented in Fig. 1, we use laser-cooled ensemble of  $N = 10^8$  Rb-87 atoms inside a magneto-optical trap (MOT) (OD=40, for details see [33]). In a typical experimental sequence, repeated synchronously with the 50 Hz SLM refresh rate, the atoms are first cooled and trapped for 19.6 ms and then the MOT coils are turned off to allow for 300  $\mu\text{s}$  cooling in optical molasses, so the ensemble can reach final temperature of 22  $\mu\text{K}$  [33]. Residual magnetic fields from eddy currents decay after 100  $\mu\text{s}$ . Once the MOT is fully switched off we pump the atoms to the  $5^2S_{1/2}, F = 1$  state with  $\langle F_x \rangle = 1$ . Then, after 100  $\mu\text{s}$  of atomic spins rotation driven only by an external magnetic field  $\mathbf{B} = B\hat{\mathbf{e}}_z$  with amplitude  $B = 100$  mG, we illuminate atomic ensemble with circularly polarized ac-Stark beam. The beam is far-detuned from the  $5^2S_{1/2}, F = 1 \rightarrow 5^2P_{3/2}, F = 2$  atomic transition and propagates along the  $z$  direction. This experimental configuration results in the net magnetic field  $\mathbf{B}_{\text{eff}} = \mathbf{B} + \mathbf{B}_f$  pointing along the  $z$  axis.

Average spin projection  $\langle \hat{F}_x \rangle$  onto the  $x$  axis is measured by registering polarization rotation of a weak linearly polarized probe beam propagating along the  $x$  direction, using a Wollaston prism and a differential photodiode (DPD) [31]. The probe beam of 1  $\mu\text{W}$  power is detuned by 100 MHz from the  $5^2S_{1/2}, F = 1 \rightarrow 5^2P_{3/2}, F = 2$  transition, minimizing the deleterious effect of incoherent excitations and tensor interaction. To avoid spin decoherence due to intensity inhomogeneities of the ac-Stark beam we correct the spatial profile using a phase-only reflective SLM and a polarizing beamsplitter (PBS). The surface of the SLM is imaged on the atomic ensemble (MOT) as well as onto a CCD camera situated in an auxiliary image plane of the SLM. This allows for direct calibration of light intensity [34] incident on the atomic ensemble. With ray-trace modelling we estimate the spatial resolution of imaging the SLM surface onto the atomic

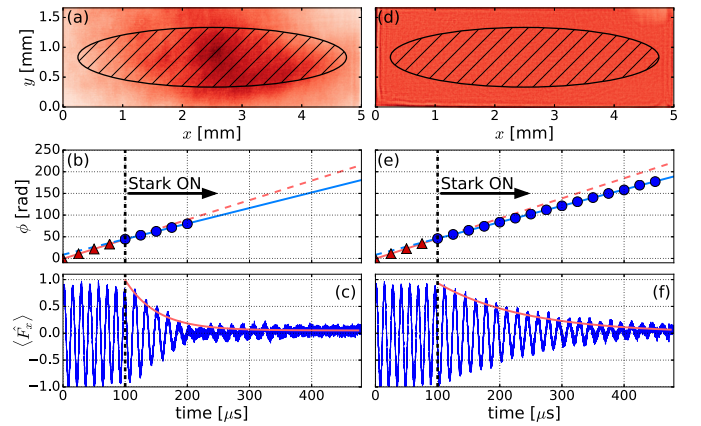


**Fig. 2.** Influence of the ac-Stark beam intensity inhomogeneity on the FID lifetime  $\tau$  for  $B_{\text{eff}} = B - B_f$ . (a) Intensity distribution  $I_0$  of  $\sigma_-$ -polarized ac-Stark beam registered on the CCD camera, without SLM correction. The shaded ellipse visualizes MOT position. (b) Phase  $\phi$  retrieved from the FID signal oscillations presented (along with its envelope) in (c). Triangles (dots) correspond to the phase  $\phi$  measured before (after) turning on the ac-Stark beam, along with the linear fits (error bars within data points). Analogous data for intensity distribution  $I_C$ , corrected using SLM to obtain flat profile of the beam in the MOT plane, are presented in (d)–(f).

ensemble to be  $20\ \mu\text{m}$ . The SLM imaging setup is switched between CCD camera and MOT using a flip mirror (FM).

As the sign of the fictitious magnetic field  $\mathbf{B}_f$  changes with the light polarization (Eq. (4)), the value of the effective magnetic field  $B_{\text{eff}}$  is the sum or the difference of  $B$  and  $B_f$ . In Fig. 2 the influence of the ac-Stark effect (with  $\Delta = -2\pi \times 30\ \text{GHz}$ ) on the typical spin-precession signal (FID) is presented for the case where the fictitious magnetic field  $\mathbf{B}_f$  of amplitude  $B_f = 20\ \text{mG}$  is subtracted from the real magnetic field  $\mathbf{B}$ . Using standard Hilbert transform method we retrieve the phase and envelope of the measured FID signal. This allows to recover only the essential parameters with high precision without fitting of the full sinusoidal FID signal. In the left column of Fig. 2 we plot the spatial intensity profile  $I_0$  of the ac-Stark beam without any SLM correction procedure (a), total accumulated phase of the FID signal (b), and the FID signal itself (c). The right column (d)–(f) portrays corresponding data for the spatial intensity profile  $I_C$  already corrected with the SLM. The average intensity of  $160\ \text{mW}/\text{cm}^2$  is selected so that the mean FID frequency shift is the same for both  $I_C$  and  $I_0$  intensity profiles. When the ac-Stark beam is applied, much shorter lifetime  $\tau$  is observed for the uncorrected, highly inhomogeneous case (Fig. 2(c)).

To explain the inherently finite lifetime  $\tau$  of the spin-precession signal let us now consider the three most essential sources of decoherence for the case of ac-Stark shift spin control. The first type is any kind of spin decoherence occurring even without the ac-Stark beam. This includes dephasing due

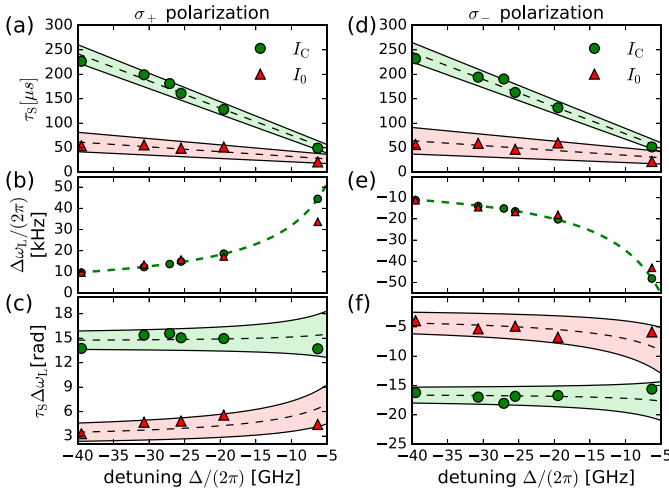


**Fig. 3.** Dependence of the FID signal on the detuning  $\Delta$  for the ac-Stark beam intensity profile with ( $I_C$ ) and without ( $I_0$ ) SLM correction. Measured ac-Stark induced dephasing lifetime  $\tau_S$  along with a fitted function (dashed line) (a), Larmor frequency shift  $\Delta\omega_L$  (b) and total phase  $\phi_S = \tau_S\Delta\omega_L$  (c) accumulated within spin coherence lifetime (the product of values from (a) and (b)) for  $\sigma_+$  polarization of the ac-Stark beam. Shading regions around dashed lines (theoretical fit) correspond to fitting uncertainties (determined for (a) and (c) from standard covariance matrix of the linear fit parameters). In (b) the theoretical scaling  $I/\Delta$  is marked by the dashed line for intensity  $I = 160\ \text{mW}/\text{cm}^2$  (errorbars within data points). Analogous quantities for  $\sigma_-$  polarization of the ac-Stark beam are plotted in (d)–(f). Maximum achievable frequency shift presented here corresponds to a fictitious magnetic field with amplitude  $B_f = 70\ \text{mG}$ .

to magnetic field inhomogeneities (occurs at a rate  $< 1\ \text{kHz}$  thus negligible in further analysis) and most importantly interaction of atoms with the probe beam, particularly the tensor interaction (Eq. (2)) which might be significant. Minimizing this effect using weak probe light (ca. microwatt power) detuned by  $100\ \text{MHz}$  from the  $5^2S_{1/2}, F = 1 \rightarrow 5^2P_{3/2}, F = 2$  transition, we obtain the FID lifetime (for  $\omega_L = 2\pi \times 74\ \text{kHz}$ ) of about  $\tau_0 = 700\ \mu\text{s}$ . The second source – associated with the manipulation itself, is an absorption and subsequent re-emission of light caused by the ac-Stark beam quantified by the scattering rate  $\Gamma_{\text{scatt}}$ . This effect is proportional to  $I/\Delta^2$  [18] while the Larmor frequency behaves as  $I/\Delta$  (Eq. (5)), therefore the way to minimize incoherent scattering is to increase  $\Delta$  and  $I$  proportionally. The last, significant source of decoherence is the dephasing caused by the intensity inhomogeneities of the ac-Stark laser beam characterized by the lifetime  $\tau_S$ , calculated as  $1/\tau_S = 1/\tau - 1/\tau_0$ .

As shown in Fig. 2, SLM-corrected ac-Stark beam intensity distribution  $I_C$  increases the FID lifetime  $\tau$  significantly compared to the situation with uncorrected intensity profile  $I_0$ . To explicitly confirm this, we plot in Fig. 3 the lifetime  $\tau_S$  along with a fit to a simple relation  $\tau_S \propto |\Delta|$ , ac-Stark induced Larmor frequency shift  $\Delta\omega_L$  and phase accumulated within the FID lifetime  $\phi_S = \tau_S\Delta\omega_L$ , as a functions of ac-Stark beam detuning  $\Delta$ . Two columns depict results for both  $\sigma_+$  and  $\sigma_-$  polarized ac-Stark light. The uncorrected ac-Stark beam mean intensity is chosen to preserve the same FID frequency as with corrected beam profile. Figure 3 (b) and (e) confirm the theoretical prediction  $\Delta^{-1}$  given by Eq. (4). The curve fitted to data corresponds to average light intensity  $I = 160\ \text{mW}/\text{cm}^2$  which is consistent with an independent measurement of light power. The total phase  $\phi_S$  accumulated within FID lifetime exhibits nearly  $\Delta$ -independent behavior which indeed confirms the dominant role of the ac-Stark shift inhomogeneities on the decoherence phenomenon. Most importantly, thanks to homogenization the possible phase  $\phi_S$  that the spin can accumulate within one  $1/e$  characteristic lifetime  $\tau_S$  increases from  $\phi_S = 5\ \text{rad}$  to about  $\phi_S = 15\ \text{rad}$  for both  $\sigma_+$  and  $\sigma_-$  polarizations of the ac-Stark beam. It is more than enough to manipulate spin pattern in an arbitrary way.

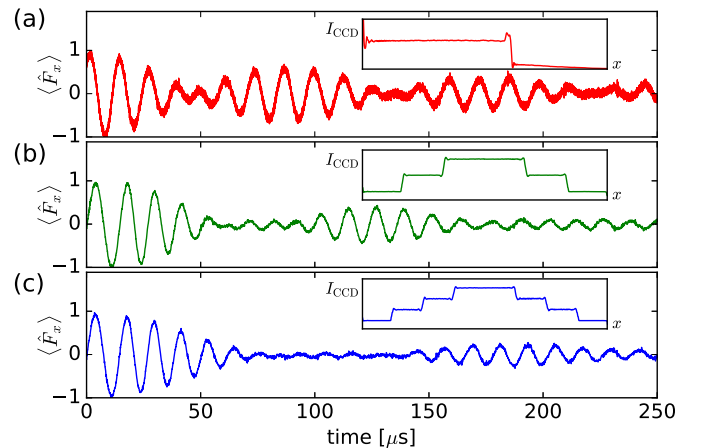


**Fig. 4.** Temporal dynamics of the FID signal for staircase intensity profile  $I_{\text{CCD}}$  registered on the CCD camera. Measured beat-note FID signal for two intensity steps (a) as well as collapse-and-revival FID signal for three (b) and four (c) intensity steps. Intensity patterns (insets)  $I_{\text{CCD}}$  are uniform in the  $y$  direction on the CCD camera.

The manipulation of atomic spins using the ac-Stark effect (fictitious magnetic field  $\mathbf{B}_f$ ) has many advantages over using only real magnetic field  $\mathbf{B}$ . First, it gives us better temporal precision in the experiment, as using the acousto-optic modulator (AOM) we can turn on/off the light in ca. hundred nanoseconds, which is impossible in case of the even low-inductance magnetic coils. Second, using SLM we can easily sculpt the intensity  $I_C$  of the ac-Stark beam into arbitrary shapes – one particular example is depicted in Fig. 4. Here atoms are illuminated with the staircase spatially-modulated ac-Stark beam (with  $\Delta = -2\pi \times 30$  GHz), visualized as cross-sections  $I_{\text{CCD}}$  of intensity profiles on the CCD camera. Thus, several groups of spins oscillate with equidistant frequencies, forming a frequency comb. With more intensity steps, or equivalently with more teeth in the frequency comb, we can achieve lower ratio of the revival duration to the time where the FID signal is collapsed, which scales linearly with the number of teeth. For only two-intensity levels (Fig. 4 (a)) the FID signal has a cosine envelope and collapses only for a moment, but for four-level staircase (Fig. 4 (c)) the FID signal almost completely disappears for about 80  $\mu\text{s}$ .

To conclude, we have demonstrated spatially-resolved control of the fictitious magnetic field generated using the ac-Stark effect. We have shown that inhomogeneities of the ac-Stark beam are the main source of dephasing. After homogenization using SLM we have achieved a phase shift of over 15 rad within the  $1/e$  lifetime of the spin coherence, which is several times longer than without spatial intensity corrections. We have also presented the possibility to engineer complex temporal dynamics of the FID signal by sculpting the ac-Stark beam intensity, from frequency shift through beat-note, to collapse-and-revival behavior. The control over spatial and temporal aspects of light in comparison to real magnetic field makes our method very robust and useful in high-resolution magnetometry [12], magnetic gradiometry [13] or spin wave manipulations [18], giving prospects to readily improve the sensitivity and precision.

**Funding.** Narodowe Centrum Nauki (NCN) (2015/19/N/ST2/01671, 2016/21/B/ST2/02559, 2017/25/N/ST2/01163 and 2017/25/N/ST2/00713); Ministerstwo Nauki i Szkolnictwa Wyższego (MNiSW) (DI2013 011943 and DI2016 014846).

**Acknowledgment.** The authors thank M. Jachura and M. Semczuk for careful reading the manuscript as well as K. Banaszek for generous support.

## REFERENCES

1. C. G. Yale, B. B. Buckley, D. J. Christle, G. Burkard, F. J. Heremans, L. C. Bassett, and D. D. Awschalom, *Proc. Natl. Acad. Sci. U.S.A.* **110**, 7595 (2013).
2. T. Moriyasu, D. Nomoto, Y. Koyama, Y. Fukuda, and T. Kohmoto, *Phys. Rev. Lett.* **103**, 213602 (2009).
3. M. Goryca, M. Koperski, P. Wojnar, T. Smoleński, T. Kazimierczuk, A. Golnik, and P. Kossacki, *Phys. Rev. Lett.* **113**, 227202 (2014).
4. D. E. Reiter, T. Kuhn, and V. M. Axt, *Phys. Rev. Lett.* **102**, 177403 (2009).
5. A. Stupakiewicz, K. Szerenos, D. Afanasiev, A. Kirilyuk, and A. V. Kimel, *Nature* **542**, 71 (2017).
6. C. Cohen-Tannoudji and J. Dupont-Roc, *Phys. Rev. A* **5**, 968 (1972).
7. C. Y. Park, H. Noh, C. M. Lee, and D. Cho, *Phys. Rev. A* **63**, 325121 (2001).
8. E. Zhivun, A. Wickenbrock, B. Patton, and D. Budker, *Appl. Phys. Lett.* **105**, 192406 (2014).
9. Z. Lin, X. Peng, W. Li, H. Wang, and H. Guo, *Opt. Express* **25**, 7668 (2017).
10. W.-M. Sun, Q. Huang, Z.-J. Huang, P.-W. Wang, and J.-H. Zhang, *Chin. Phys. Lett.* **34**, 058501 (2017).
11. M. Vengalattore, J. M. Higbie, S. R. Leslie, J. Guzman, L. E. Sadler, and D. M. Stamper-Kurn, *Phys. Rev. Lett.* **98**, 200801 (2007).
12. M. Koschorreck, M. Napolitano, B. Dubost, and M. W. Mitchell, *Appl. Phys. Lett.* **98**, 074101 (2011).
13. A. B. Deb, B. J. Sawyer, and N. Kjærgaard, *Phys. Rev. A* **88**, 1 (2013).
14. P. R. Hemmer and T. Zapata, *J. Opt.* **14**, 083002 (2012).
15. N. Goldman, G. Juzeliūnas, P. Öhberg, and I. B. Spielman, *Rep. Prog. Phys.* **77**, 126401 (2014).
16. M. Rosatzin, D. Suter, and J. Mlynek, *Phys. Rev. A* **42**, 1839 (1990).
17. M. Zielonkowski, J. Steiger, U. Schünemann, M. DeKieviet, and R. Grimm, *Phys. Rev. A* **58**, 3993 (1998).
18. B. M. Sparkes, M. Hosseini, G. Hétet, P. K. Lam, and B. C. Buchler, *Phys. Rev. A* **82**, 043847 (2010).
19. T. Chanelière and G. Hétet, *Opt. Lett.* **40**, 1294 (2015).
20. C. Y. Park, J. Y. Kim, J. M. Song, and D. Cho, *Phys. Rev. A* **65**, 033410 (2002).
21. P. Schneeweiss, F. Le Kien, and A. Rauschenbeutel, *New J. Phys.* **16**, 013014 (2014).
22. B. Albrecht, Y. Meng, C. Clausen, A. Dareau, P. Schneeweiss, and A. Rauschenbeutel, *Phys. Rev. A* **94**, 061401(R) (2016).
23. M. Parniak and W. Wasilewski, *Phys. Rev. A* **91**, 023418 (2015).
24. A. Leszczyński, M. Parniak, and W. Wasilewski, *Opt. Express* **25**, 284 (2016).
25. X.-W. Zhang, A. Kalachev, P. Hemmer, M. O. Scully, and O. Kocharovskaya, *Laser Phys.* **24**, 094016 (2014).
26. M. Mazelanik, M. Dąbrowski, and W. Wasilewski, *Opt. Express* **24**, 21995 (2016).
27. M. Parniak, A. Leszczyński, and W. Wasilewski, *Phys. Rev. A* **93**, 053821 (2016).
28. S. de Echaniz, M. Koschorreck, M. Napolitano, M. Kubasik, and M. W. Mitchell, *Phys. Rev. A* **77**, 032316 (2008).
29. A. Smith, B. E. Anderson, S. Chaudhury, and P. S. Jessen, *J. Phys. B* **44**, 205002 (2011).
30. N. Behbood, F. Martin Ciurana, G. Colangelo, M. Napolitano, M. W. Mitchell, and R. J. Sewell, *Appl. Phys. Lett.* **102**, 173504 (2013).
31. J. M. Geremia, J. K. Stockton, and H. Mabuchi, *Phys. Rev. A* **73**, 042112 (2006).
32. G. Colangelo, R. J. Sewell, N. Behbood, F. M. Ciurana, G. Triginer, and M. W. Mitchell, *New J. Phys.* **15**, 103007 (2013).
33. M. Parniak, M. Dąbrowski, M. Mazelanik, A. Leszczyński, M. Lipka, and W. Wasilewski, *Nat. Commun.* **8**, 2140 (2017).
34. A. Leszczyński and W. Wasilewski, *J. Opt. Soc. Am. A* **33**, 683 (2016).